

*SET Technical Report SET\_TR2006-002*

**A Summary of SOLAR 0.1-0.8nm X-ray Measurements From  
the GOES Satellites, 1986-2004**

Dave Bouwer, Space Environment Technologies

April 18, 2006

## **Table of Contents**

Introduction	3
The GOES Spacecraft and XRS	5
The X-ray Xi, Background Xb10, and Flare Xhf Indices	7
Data Summary	11
Inter-Comparisons of GOES Satellites	16
Case Study: Xb10 compared to F10.7	19
Case Study: The Halloween Flares	21
Conclusions	22
Appendix A. Glossary Acknowledgments	23

## Introduction

A new technique for determining the background X-ray 0.1-0.8 nm flux, and the flares above a background, has been developed for space weather applications. This report begins with a brief discussion of the GOES X-ray 0.1-0.8 nm data, the GOES spacecraft, and the X-ray sensor (XRS) instrument. All historical GOES X-ray data (often referred to as the 1-8 Å X-ray flux) from 1986 to 2004 was retrieved from the NGDC SPIDR database, validated, and converted to daily background  $X_{b10}$  and hourly flare  $X_{hf}$  indices. Next, the derivations of the  $X_{b10}$  and  $X_{hf}$  indices are described, and a summary of the derived data are presented. Additionally, results of the comparisons between the different GOES satellites when there are concurrent data are presented, addressing satellite-to-satellite calibrations. Finally, two case studies implementing the  $X_{b10}$  and  $X_{hf}$  are described.

One of the goals of the re-analysis of the X-ray data and development of background and flare indices was to develop useful proxies for studies in thermospheric and ionospheric phenomena. This report focuses primarily on the long-term X-ray variations; the variations due to the solar cycle (years), active region evolution (months), and solar rotation (weeks). Recently a solar flare evolution prediction model based on the X-ray indices presented here has been implemented at the Space Environment Technologies <http://www.SpaceWx.com> website (Tobiska, W.K. and S.D. Bouwer, "Solar flare evolution model for operational users," IES2005 Proceedings, ed. J.M. Goodman, in press, 2005), and (Tobiska, W.K., "Systems-Level Space Environment Specification for Satellite and Ground System Operations", American Institute of Aeronautics and Astronautics, Inc., 2005).

X-rays are an important source for ionization in the D-region of the ionosphere, affecting radio communication, GPS operations, and other technological systems. To the extent soft X-ray (XUV) and extreme ultraviolet (EUV) solar irradiances are correlated with X-ray irradiance, thermospheric heating can be better estimated, and this has important implications to satellite drag and other operations. Since many geomagnetic indices and operational requirements use one-hour and daily indices, an the initial analysis described in this report uses hourly and daily cadences. However, two by-products of these data, the daily minimum background,  $X_{b10}$ , showing intermediate term active region evolution and the hourly flare index,  $X_{hf}$ , showing flare shapes can provide new insights in solar physics research and be useful for operational predictions as well.

Figure 1 shows 3 days of the 5-minute X-ray flux measurements. These data are used by NOAA/SEC to officially classify flares, and are the GOES/XRS measurements of the X-ray energy that is responsible for many ionospheric and thermospheric phenomena. This figure is one of the most familiar in the space-weather community, and illustrates the integrated effect of flares combined with background.

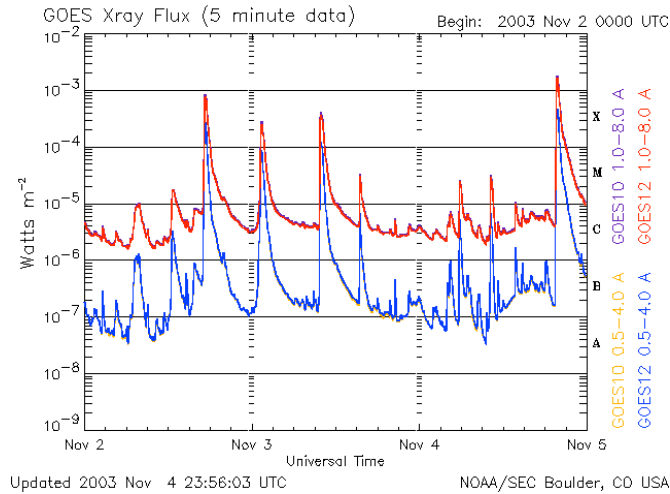


Figure 1. The GOES X-ray data as it is operationally presented by the NOAA Space Environment Center (NOAA/SEC)

Figure 2 illustrates some of the physical conditions associated with solar X-ray irradiance. The million-degree temperatures and intense magnetic fields present in the corona cause irradiances at the low-wavelength end of the spectrum to vary by orders of magnitude. The active regions dominate the data, and evolve over days to months. Flares above the active regions vary on the order of minutes to hours. A fainter, but ever-present background corona extends beyond the photosphere and chromosphere of the Sun, except in coronal hole regions. X-ray irradiances are optically thin and as a result, from a terrestrial view there is no attenuation of coronal emissions due to their longitudinal central-meridian distance (CMD) and large loops above the active region are visible even when the lower region has rotated well-past the limb.

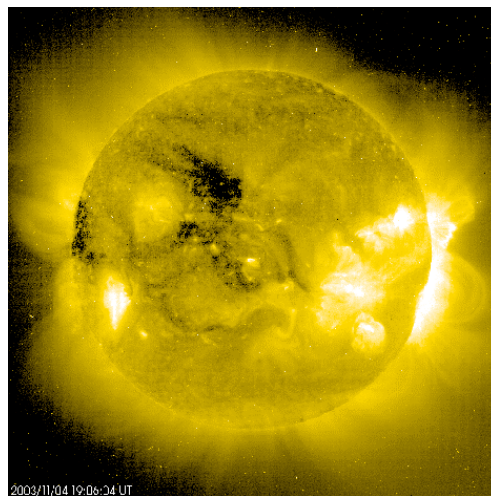


Figure 2. The solar corona as seen by the SOHO/EIT satellite imager on November 4, 2004, looking at the Fe XV 28.4 nm line.

## The GOES Spacecraft and XRS

The operational 0.1-0.8 nm X-ray measurements began with the SMS-2 satellite in 1975, and have continued with geo-synchronous GOES 1-12 satellites since then. There are usually two GOES satellites operational at all times, separated in longitude and providing two concurrent sets of data with the exception of eclipse conditions discussed below. Primarily for terrestrial weather imagery, the GOES satellites also carry space environment instruments to measure geomagnetic, particle, and X-ray variations. This report focuses only on the X-ray sensor (XRS) data from 1986 to the present.

The GOES series of satellites are described in greater detail are at:

<http://rsd.gsfc.nasa.gov/goes/text/goes.databook.html>.

Detailed descriptions of the SEM instruments, particularly the X-ray sensor (XRS), are found at:

<http://www.ngdc.noaa.gov/stp/GOES/goes.html> and

[http://goes.ngdc.noaa.gov/data/GOES-8-12\\_SEMDataBook.pdf](http://goes.ngdc.noaa.gov/data/GOES-8-12_SEMDataBook.pdf)

The XRS is a whole-disc X-ray photometer that measures in real-time solar X-ray flux in the spectral range of 0.05 to 0.4 nm (short Sun channel) and 0.1 to 0.8 nm (long Sun channel) [Donnelly, R. F. R. N. Grubb, and F. C. Cowly., “Solar X Ray measurements from SMS-1, SMS-2, and GOES-1, information for data users”, NOAA Tech. Memo., ERL/SEL-48, NOAA/ERL, Boulder, CO, 1977]. The instrument has proven to be remarkably reliable, showing negligible long-term drift in sensitivity. The XRS assembly consists of a telescope collimator and sweeper magnet subassembly, dual ion chamber and preamplifier subassemblies, a DPU (data processing unit) subassembly, and a magnet subassembly. X-rays are detected by two ion chambers, one for each spectral range. The detector output signals are processed by separate electronic channels that provide automatic range selection. Nominal flux levels expected are on the order of  $2 \times 10^{-8}$  to  $2 \times 10^{-3}$  W/m<sup>2</sup> for the long channel and  $5 \times 10^{-9}$  to  $5 \times 10^{-4}$  W/m<sup>2</sup> for the short channel. The capability exists to calibrate each channel via ground command. The aperture of the XRS is provided with a pair of sweeper magnets to deflect incoming electrons away from the ion chambers so that only X-rays are admitted. The XRS is housed as a single unit on the XRS drive assembly; this combination is mounted on the solar array yoke on the side of the spacecraft body in a position that provides the XRS and drive assembly Sun sensors a clear field of view to the Sun at all times. The sampling rate of the XRS is once every 0.512 seconds, and it takes about 2 seconds to reach 90% of the final value (note that subsequent data processing adjusts the apparent discrepancies in sampling rates for the one-minute data). The satellite telemetry is received at the NOAA Space Environment Center in Boulder, Colorado, and pre-processing finally results in one- and five-minute average real-time operational data.

Prior to GOES-8, the long channel had threshold sensitivities between  $2 \times 10^{-9}$  W/m<sup>2</sup> and  $2 \times 10^{-4}$  W/m<sup>2</sup>. When GOES 8 became operational, the subsequent 3-axis stabilized spacecrafts replaced the GOES 1-7 spin stabilized satellites. Furthermore, the XRS dynamic range was increased beginning with GOES-8, resulting in a increased upper limit of approximately  $1 \times 10^{-3}$  W/m<sup>2</sup> to  $2 \times 10^{-3}$  W/m<sup>2</sup>, making it possible to better measure maximum fluxes of solar flares. Also, beginning with GOES-10, the analog-to-digital converter output was decreased from 8 to 7 bits to improve a signal noise problem; this resulted in a data quantization artifact at the lowest flux levels of the instrument, as can be seen in Figure 3.

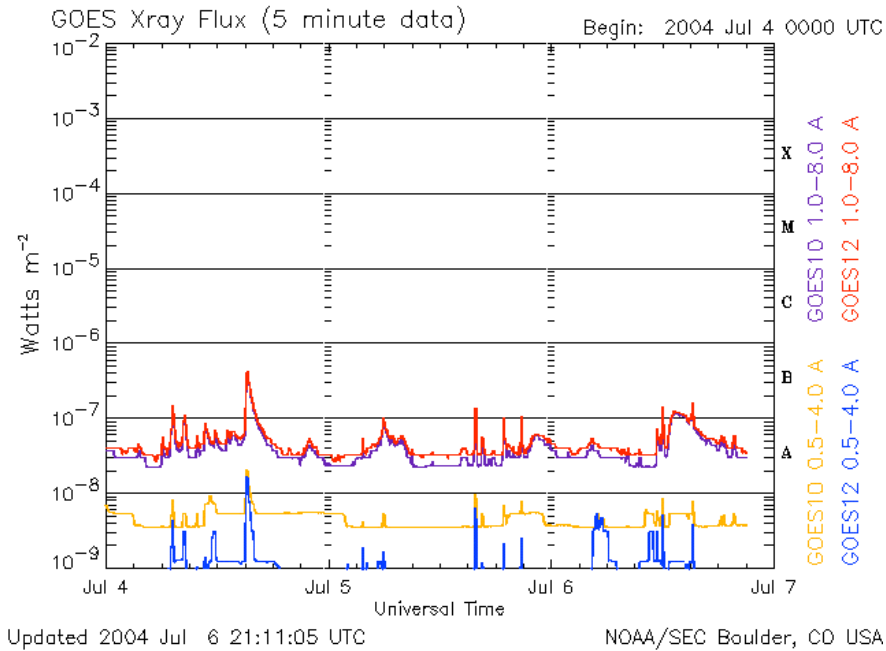


Figure 3. GOES-10 and 12 one-minute values exhibit quantization at about  $3 \times 10^{-8}$  W/m<sup>2</sup>. This effect disappears at about  $6.4 \times 10^{-8}$  and  $5.5 \times 10^{-8}$ , respectively

Figure 4 shows the resulting date range covered by each satellite from NGDC archives. Where there are vertical lines, only a portion of that year is available. GOES-11 has the same dynamic range as GOES-12 but it is currently in a parking orbit; data will not become available until another satellite becomes operational. Earlier SMS-2 and GOES 1- 3 archival data are available as FITS files, but are not included in this study.

S/C	Ndays	86	87	88	89	90	91	92	93	94	95	96	97	98	99	00	01	02	03	04	start	end			
G5	448	█	█	█	█	█	█	█	█	█	█	█	█	█	█	█	█	█	█	█	█	█	1/1/86	3/24/87	
G6	3042	█	█	█	█	█	█	█	█	█	█	█	█	█	█	█	█	█	█	█	█	█	█	1/1/86	4/30/94
G7	3203	█	█	█	█	█	█	█	█	█	█	█	█	█	█	█	█	█	█	█	█	█	█	3/6/87	8/12/96
G8	2963	█	█	█	█	█	█	█	█	█	█	█	█	█	█	█	█	█	█	█	█	█	█	3/1/95	4/10/03
G9	848	█	█	█	█	█	█	█	█	█	█	█	█	█	█	█	█	█	█	█	█	█	█	4/1/96	7/27/98
G10	2010	█	█	█	█	█	█	█	█	█	█	█	█	█	█	█	█	█	█	█	█	█	█	7/1/98	12/31/03
G12	508	█	█	█	█	█	█	█	█	█	█	█	█	█	█	█	█	█	█	█	█	█	█	1/10/03	5/31/04

Figure 4. The times covered by each GOES satellite from 1986 to 2004.

There are a number of data artifacts. GOES-9 had numerous spacecraft problems resulting in limited data and it is not used in the analysis. For the other satellites, there are occasional

spacecraft maneuvers, data processing outages, and seasonal eclipses when the Earth blocks the XRS line-of-sight view of the Sun. In most cases, these are easily detected and replaced with another satellite's daily values. Nevertheless, about 1% of the data is still missing. Recently work has been completed that replaces missing data from one satellite with another, resulting in a single X-ray time series from 1986 to 2004. This time series is now available from SET, and work is in progress to improve the sampling rate down to one minute and to make X-ray indices available operationally. This report also presents results of correlations between concurrent datasets, where each satellite's data is compared to the prior dataset in the case where both operated simultaneously.

A recurring event that results in missing data is when the Sun is eclipsed by the Earth due to the geometry of the GOES orbit. This occurs in the spring and fall and, in these periods, data drops out for up to 70 minutes. Once the satellite is back in Sunlight, the instruments quickly return to normal performance. In figure 5, a one-year time series of 1-minute cadence data at various stages of processing is illustrated. Between days 70-100, for example, many daily measurements are missing. The final X-ray time series produced by our study replaces one day's X-indices with those from another satellite when an eclipse is detected anytime during the day.

SEC operational measurements and historical databases are available from <http://www.sec.noaa.gov> website, and from the <http://ngdc.noaa.gov> website. Since most public access to the archival GOES data is through the <http://spidr.ngdc.noaa.gov/spidr/> website, those data were used in creating the X-ray database in this study.

## **The X-ray $X_i$ , Background $X_{b10}$ , and Flare $X_{hf}$ Indices**

The original concept of an X-ray index calculated from the log transformation below was first suggested by Donnelly in 1979 (private communication). Donnelly suggested this index as a way to more easily compare X-ray variations to the Ottawa F10.7 flux, while preserving a means to reverse the index into its original units. Taking the log of an exponentially-varying time series to de-emphasize the large extremes is a simple statistical technique commonly used. Figure 6 below illustrates the steps to calculate the indices from the one-minute 0.1-0.8 nm fluxes (in  $W/m^2$ ). The X-ray index  $X_i$  is calculated from the X-ray flux  $\Phi_{1-8}$ , which is in units of  $W/m^2$ , using the equation

$$X_i = 100 \times \log(\Phi_{1-8} \times 10^{10}) \quad (1)$$

This results in a dimensionless index roughly in the same range as the Penticton F10.7 index, helping in the visualization of time series and statistical comparisons. Note that all the X-indices can be converted from dimensionless solar flux units (SFU) back to solar flux  $W/m^2$  units by applying the anti-log equation

$$\Phi_{1-8} = 10^{[(X_i - 1,000) / 100]} \quad (2)$$

For example, an X-class flare exceeding  $10^{-4} W/m^2$ ,  $X_i = 600$ , for an M-class flare above  $10^{-5} W/m^2$ ,  $X_i = 500$ , and for a C-class flare above  $10^{-6} W/m^2$ ,  $X_i = 400$ . Figure 5 below illustrates these indices.

The original background X-ray index (denoted  $X_b$ ) for was introduced by Dave Bouwer et. al. in a NOAA Technical Memorandum (ERL SEL-62), 1982, and it became an operational product at NOAA/SEC soon after. That publication presented data that covered the period of 1976-1981 using SMS2 and GOES 1, 2, and 3 data. Unfortunately, a software programming error was introduced into the NOAA/SEC operational software, resulting in a background index calculated from the first two hours of the day instead of all 24 hours. This problem was not detected until 2003. Since then, the data has been removed from the NOAA/NGDC archives. One of the original motivations for this work was to correct the X-ray background indices for dissemination by NOAA SEC and NGDC. A task after developing a new X-ray database is to deliver the latest background and flare indices derived here to NGDC.

By applying a log transformation to the one-minute flux, taking the lowest decile of the hourly data, then finding the minimum hourly decile of the day, an “X-ray Daily Background Minimum Index“ (denoted  $X_{b10}$ ) is derived that appears to effectively removes the exponentially increasing flares from the time series. Compared to  $X_b$ ,  $X_{b10}$  better estimates the day-to-day variations in active regions, without the impulsive flares shorter than a days duration. The difference between the hourly median X-index and  $X_{b10}$  is used to estimate an hourly “Flare Index” (denoted  $X_{hf}$ ), representing a solar flare above the background.

As mentioned earlier, the lowest effective range imposed by the X-ray sensors and pre-processing is increasingly limited. In 1995, GOES-8 was the first of the series where the spacecraft changed from a spin-stabilized design to a three-axis stabilized design. The highest range XRS can measure was changed at that time as well from  $1 \times 10^{-3} \text{ W/m}^2$  to  $2 \times 10^{-3} \text{ W/m}^2$ , making it more able to measure the high fluxes during flares, but at the cost of detecting lower flux levels. Additionally, the telemetry was decreased from nine to eight bits. As a result, the bottom cut-off range of the XRS measurements was increased by about a decade, and results in a nearly total loss of meaningful data during solar minimum. The next event that resulted in an additional loss of the lowest valid XRS data began in 1998 with GOES-10 and GOES-12, when a small change to fix signal noise in on-board electronics resulted in energy quantization at low flux levels. Based on the lowest non-zero  $X_{b10}$  (see definition in the next section), the “basement” values of each satellite are:

Satellite	obs. min. $X_{b10}$ (unitless)	obs. min. Flux $\text{W/m}^2$	suggested min. $X_{b10}$ (unitless)	suggested min. Flux $\text{W/m}^2$
GOES-5	102.94	$1.07 \times 10^{-9}$	103	$1.1 \times 10^{-9}$
GOES-6	102.12	$1.05 \times 10^{-9}$	103	$1.1 \times 10^{-9}$
GOES-7	107.19	$1.18 \times 10^{-9}$	108	$1.2 \times 10^{-9}$
GOES-8	157.7	$3.82 \times 10^{-9}$	158	$4.0 \times 10^{-9}$
GOES-10	280.41	$6.37 \times 10^{-8}$	281	$6.4 \times 10^{-8}$
GOES-12	274.19	$5.50 \times 10^{-8}$	274	$5.5 \times 10^{-8}$

Table 1. The lowest observed flux, after the one-minute data has been converted to  $X_{b10}$ , in both the dimensionless X-index units and the flux units in  $\text{W/m}^2$ , and the suggested

minimum flux (the observed values rounded up) that should be considered the lowest-possible valid measurement.

One of the recent efforts has been the derivation of a new X-ray background index. One of the motivations was to find a background index that closely represented the minimum value of X-ray flux during a day. Since flares typically last less than 8 hours, a consistent statistical method could be used to approximate the slowly-varying active region evolution over weeks and months. While flares are of great interest from both a solar and ionospheric/thermospheric viewpoint, it is the more slowly-varying components that have the most significant impact on thermospheric and ionospheric dynamics. It was for this idea the background and flare indices were developed.

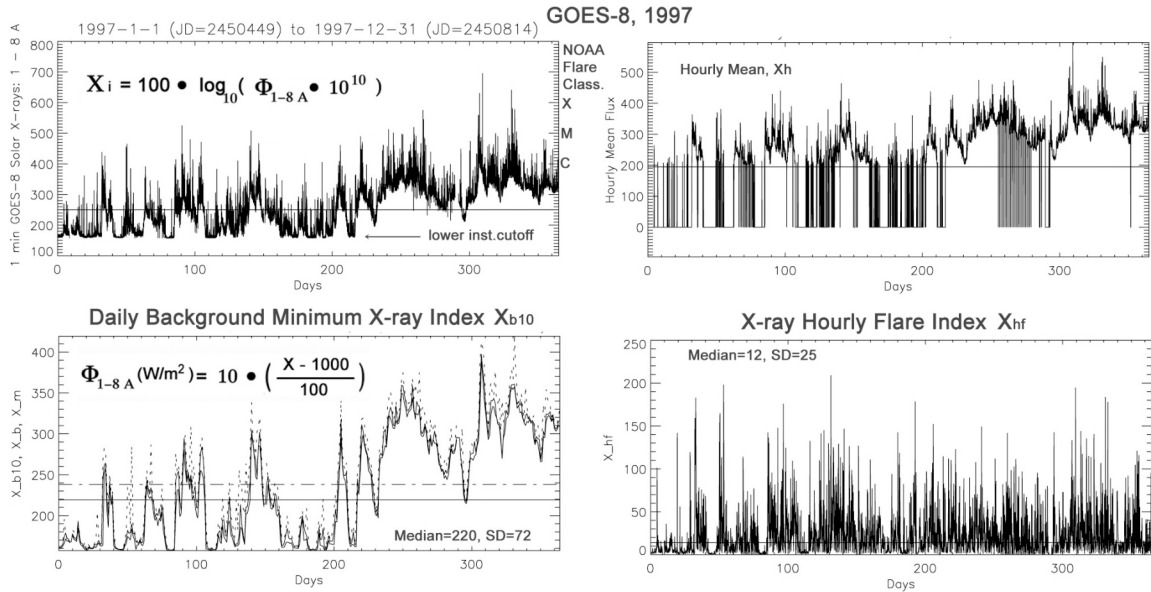


Figure 5. Four plots illustrating the derivation of the Daily Minimum Background Index  $X_{b10}$  and the Hourly Flare Index  $X_{hf}$ .

In figure 5, the top-left plot of the one-minute X-ray flux shows the range of  $X_i$ ; including where the lowest threshold of the GOES-7 instrument is ( $X_i = 158$ ). On the right y-axis label, the NOAA/SEC flare classifications are shown (X-class =  $10^{-4}$  W/m<sup>2</sup>, M-class =  $10^{-5}$  W/m<sup>2</sup>, C-class =  $10^{-6}$  W/m<sup>2</sup>), which are equivalent to  $X_i = 600, 500,$  and  $400,$  respectively. The top-right plot is for illustration; it is the hourly means (0.0 is the missing-value flag, and appears in the plot as such to visually emphasize missing data), which are nearly identical to the hourly median values used later, except when there are missing data. It is not unusual to have large data spikes due to solar flares in the one-minute data, and using the median instead of the mean mitigates the effect of large flux values dominating the hourly value. The bottom-left plot is of  $X_{b10}, X_b,$  and the daily median. The solid and dashed horizontal lines are the years median and mean, respectively. On this scale, the differences between  $X_{b10}$  and  $X_b$  are scarcely noticeable (see figure 6.) Finally, the bottom-right plot is the hourly flare index  $X_{hf}$ , which is calculated by taking the difference between the hourly median and daily background.

## How the Background X indices are Calculated

The old background X-ray index introduced in 1982,  $X_b$ , was calculated using the following algorithm:

- (1) Divide 24 hourly averages into three equal “bins” of 8 hours.
- (2) Select the minimum hourly average from each bin (using the data in  $W/m^2$  units).
- (3) Perform a simple linear interpolation between the minima of the outside bins for an interpolated minimum halfway (in time) between the outside minima.
- (4) Select the lower minimum from either the middle bin or the interpolated minimum, and convert to the X-ray index using  $X_b = 100 \times \log(\Phi \times 10^{10})$ . This selected mid-day minimum is defined as the daily background X-ray flux.

The new daily minimum background X-ray index,  $X_{b10}$ , is calculated using the following algorithm (which may need to be changed in the future to account for changes in instrument behavior or data processing):

- (1) Convert the X-ray flux measurements,  $\Phi$ , from  $W/m^2$  to the dimensionless  $X_i$  units using  $X_i = 100 \times \log(\Phi \times 10^{10})$
- (2) Calculate the lower decile from each hour’s data. The decile is calculated by sorting the 60 non-zero one-minute values and selecting the  $1/6^{\text{th}}$  data value from the bottom of the sorted list. If there are less than 20 non-zero values, the hour is flagged as missing.
- (3) Calculate the minimum from the days 24 decile values. This minimum of the day’s hourly decile values is defined as the daily minimum background X-ray index,  $X_{b10}$ .

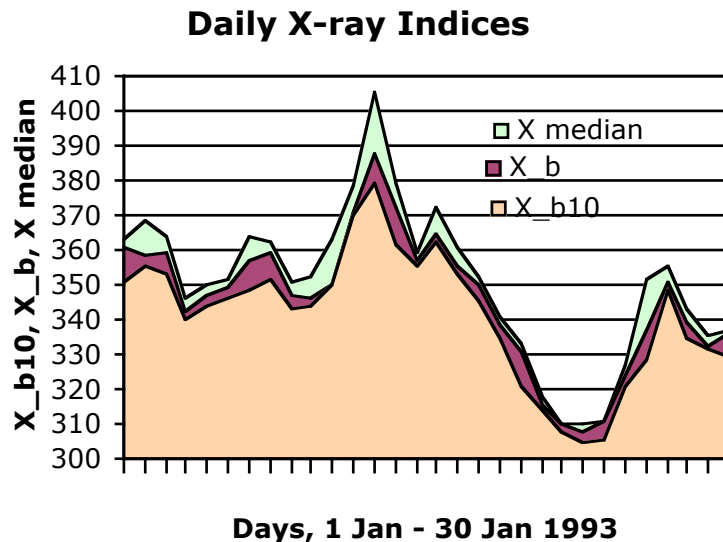


Figure 6. Daily X-ray indices. The relative improvement in estimating the daily minimum background index can be seen by comparing it to the 1982 daily background index and the median of the day’s hourly median values.

## Data Summary

One utility of our approach is that from a thermospheric and ionospheric viewpoint, dramatic relative changes in solar ionizing irradiances above the gradual day-to-day variations are often needed, as opposed to the absolute fluxes (e.g., TEC variations that last on the order of an hour). Conversely, the longer duration of day-to-day variations may have implications to the more gradual thermospheric changes (e.g., thermospheric heating, recombination, winds, etc.).

SEC operational measurements and historical databases are available from <http://www.sec.noaa.gov> website, and from the <http://ngdc.noaa.gov> website. Since most public access to the archival GOES data is through the <http://spidr.ngdc.noaa.gov/spidr/> website, that data was used in creating an SET X-ray database.

Combining the individual data tables results in over 18 years of data, as shown in figure 7, shows  $X_{b10}$  and  $X_{hf}$  over 18 years; nearly two solar cycles. In  $X_{b10}$ , the effects of the solar cycle, active region evolution, and solar rotation are apparent. Note that when GOES-8 became operational during solar minimum, the change in the lowest range is apparent during 1994-1995.

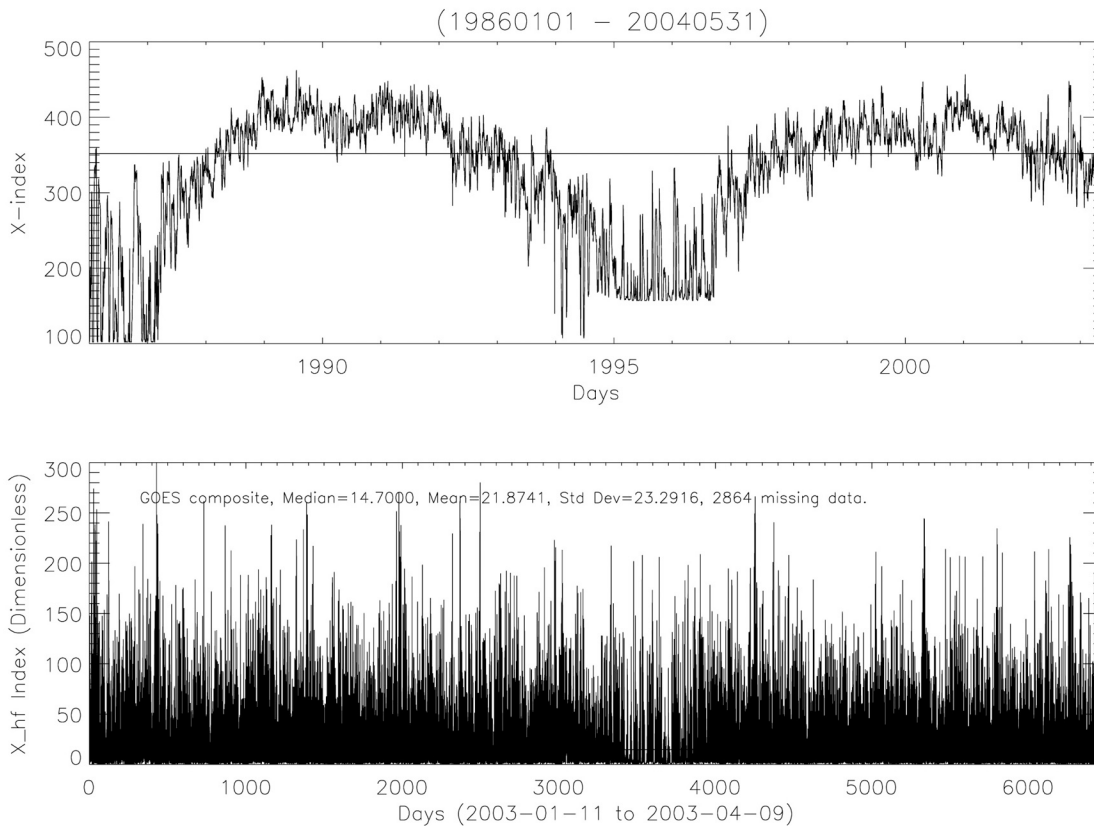


Figure 7.  $X_{b10}$  and  $X_{hf}$  from Jan 1, 1986 to May 31, 2004. The median value of  $X_{b10} = 352$ . for all data is plotted in the top panel.  $X_{hf} > 0.0$  is plotted in the bottom panel.

However, we know from an error analysis (see “Inter-comparisons of GOES Satellites” section below) that the data becomes unreliable or simply unavailable below about  $X_{b10} < 200$  (The GOES-8 bottom range is at about  $X_{b10} = 158$ , GOES-7 at 108, and GOES-5 and GOES-6 at 103, and but we are being conservative because of large errors at low flux levels). As a visual aid, the results of removing the lowest ranges of the satellites for one consistent time series are shown below in figure 8.

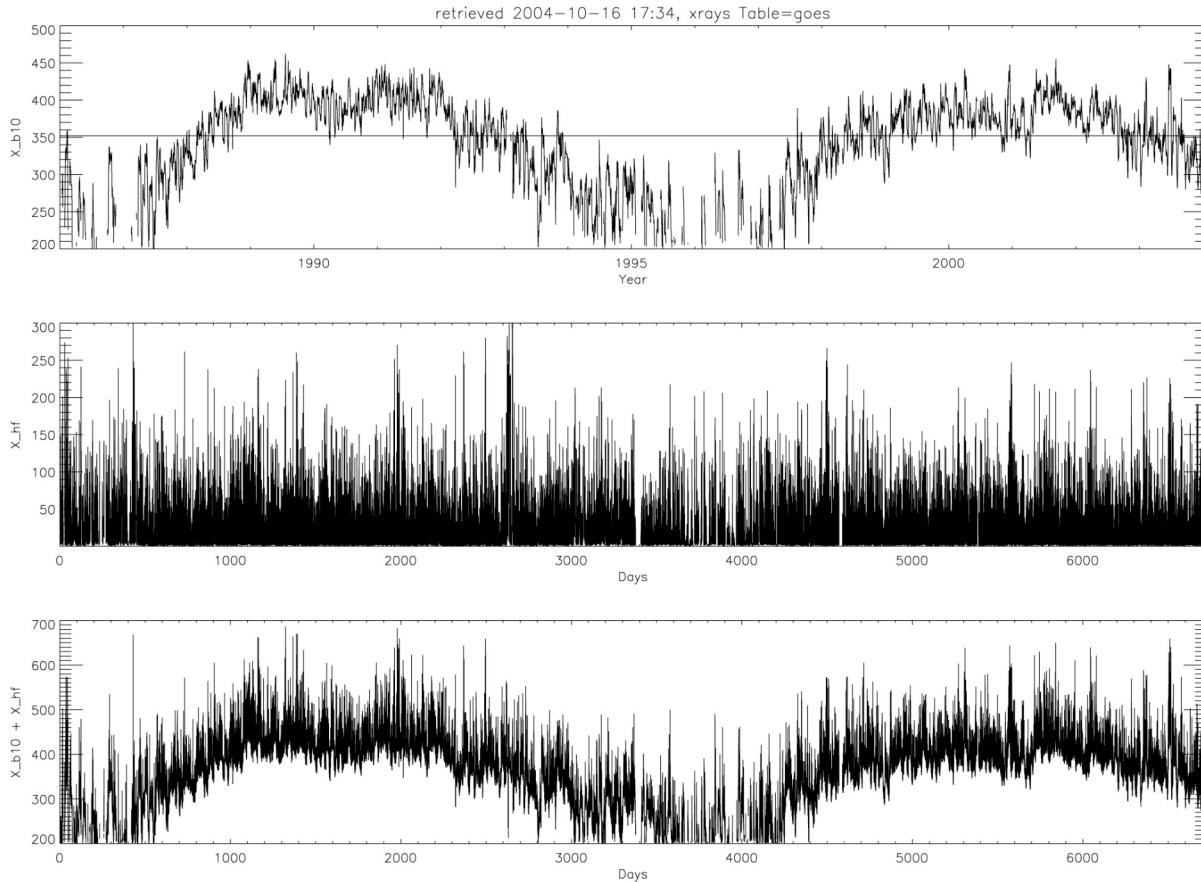


Figure 8. Adjusting for instrument limits and measurement noise, the 1986-2004 solar X-ray daily background minimum,  $X_{b10}$ , and the flare index,  $X_{hf}$ , and the sum of  $X_{b10}$  and  $X_{hf}$ . The daily X-index input data mean = 328.910, median = 351.850, min = 103.340, max = 462.430, standard deviation = 77.8281. The daily  $X_{hf}$ -index input data mean = 22.2156, median = 15.1000, min = 0.0, max = 458.800, standard deviation = 23.1608

The most striking feature in figures 7 and 8 is the apparent randomness of  $X_{hf}$ . A detailed analysis is beyond the scope of this report, but it is known  $X_{hf}$  has virtually no significant periodicities that persist past active-region lifetimes of 4.5 solar rotations (Bouwer, S. D., “Intermediate-Term Epochs in Solar Soft X Ray Emission”, J. Geophys. Res., 88, 7823-7830, 1983).  $X_{hf}$  flares occur randomly, and during solar minimum a flare above the background is typically as large as they are during solar maximum. Because there are more large active regions

during solar maximum, more flares are observed, but they all appear with a random log-normal distribution. Figure 9 below shows an example using the GOES-12 2003 data.

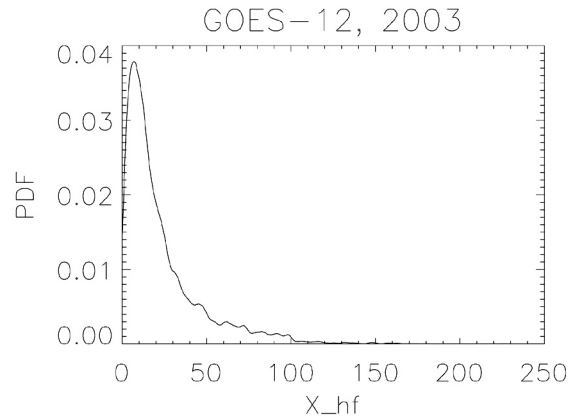


Figure 9. The probability density function for the GOES-12 2003  $X_{hf}$  data.

Extracting all  $X_{hf}$  values above 200, 75 potential flares have been identified. Table 2 below lists flares, and we see that the largest flare occurred Mar 6, 1987, with a maximum  $X_{hf}$  = 458.8. In comparison, the largest X-class flare recorded on November 2, 2003 had an  $X_{hf}$  of only 218.4.

$X_{hf} > 200.0$ , Sorted by Date			$X_{hf} > 200.0$ , Sorted by $X_{hf}$	
Date	max $X_{hf}$		Date	max $X_{hf}$
16-Jan-1986	201.6	1	6-Mar-1987	458.8
28-Jan-1986	274.2	2	8-Apr-1993	367.8
6-Feb-1986	238.6	3	20-Mar-1993	362.7
7-Feb-1986	232.7	4	7-Apr-1993	312.1
14-Feb-1986	222.5	5	9-Mar-1993	282.8
17-Feb-1986	253.6	6	2-Nov-1992	280.2
4-May-1986	241.4	7	9-Apr-1993	279.7
9-Dec-1986	239.1	8	8-Mar-1993	277.3
6-Mar-1987	458.8	9	28-Jan-1986	274.2
8-Mar-1987	248.2	10	1-Jun-1991	270.9
13-Mar-1987	239.4	11	27-Apr-1998	266.4
2-Jan-1988	261.6	12	16-Mar-1993	263.2
17-May-1988	237.6	13	2-Jan-1988	261.6
24-Jun-1988	212.6	14	25-Jun-1992	261.6
6-Mar-1989	227.8	15	19-Oct-1989	260.2
10-Mar-1989	238.3	16	17-Feb-1986	253.6
16-Aug-1989	223.7	17	18-May-1991	251.7
17-Aug-1989	207.1	18	23-Apr-1998	249.4
29-Sep-1989	233.7	19	24-Oct-1989	248.3
19-Oct-1989	260.2	20	8-Mar-1987	248.2
22-Oct-1989	201.8	21	12-Apr-2001	246.9
24-Oct-1989	248.3	22	28-Jun-1992	244.7

30-Nov-1989	217.2	23	13-Mar-1993	244.6
18-May-1991	251.7	24	24-Aug-1998	244.1
1-Jun-1991	270.9	25	4-May-1986	241.4
4-Jun-1991	231.6	26	29-Apr-1998	240.4
6-Jun-1991	231.6	27	13-Mar-1987	239.4
11-Jun-1991	206.4	28	9-Dec-1986	239.1
15-Jun-1991	237.8	29	6-Feb-1986	238.6
8-May-1992	229.7	30	10-Mar-1989	238.3
25-Jun-1992	261.6	31	15-Jun-1991	237.8
28-Jun-1992	244.7	32	17-May-1988	237.6
30-Oct-1992	231.2	33	20-Jul-2002	237.0
2-Nov-1992	280.2	34	29-Sep-1989	233.7
8-Mar-1993	277.3	35	7-Feb-1986	232.7
9-Mar-1993	282.8	36	4-Jun-1991	231.6
13-Mar-1993	244.6	37	6-Jun-1991	231.6
16-Mar-1993	263.2	38	27-Mar-1993	231.3
20-Mar-1993	362.7	39	30-Oct-1992	231.2
22-Mar-1993	229.0	40	10-Apr-2001	231.1
27-Mar-1993	231.3	41	8-May-1992	229.7
7-Apr-1993	312.1	42	22-Mar-1993	229.0
8-Apr-1993	367.8	43	6-Mar-1989	227.8
9-Apr-1993	279.7	44	16-Jun-2003	226.4
10-Apr-1994	213.3	45	28-Oct-2003	225.9
29-Aug-1994	201.8	46	16-Aug-1989	223.7
11-Sep-1994	213.2	47	14-Feb-1986	222.5
20-Oct-1995	217.4	48	23-Jul-2002	221.8
11-Mar-1996	202.1	49	28-May-2003	220.4
5-May-1996	208.2	50	15-Apr-2001	218.7
22-Aug-1996	206.2	51	25-Aug-2001	218.0
12-May-1997	209.0	52	2-Nov-2003	217.9
23-Apr-1998	249.4	53	20-Oct-1995	217.4
27-Apr-1998	266.4	54	30-Nov-1989	217.2
29-Apr-1998	240.4	55	24-Aug-2002	214.0
18-Aug-1998	202.5	56	6-Jun-2000	213.4
24-Aug-1998	244.1	57	10-Apr-1994	213.3
28-Nov-1998	210.5	58	11-Sep-1994	213.2
6-Jun-2000	213.4	59	24-Jun-1988	212.6
10-Apr-2001	231.1	60	22-Nov-2001	211.7
12-Apr-2001	246.9	61	21-Apr-2002	211.6
15-Apr-2001	218.7	62	18-Mar-2003	211.2
25-Aug-2001	218.0	63	28-Nov-1998	210.5
24-Sep-2001	208.2	64	12-May-1997	209.0
22-Nov-2001	211.7	65	5-May-1996	208.2

28-Dec-2001	207.9	66	24-Sep-2001	208.2
21-Apr-2002	211.6	67	28-Dec-2001	207.9
20-Jul-2002	237.0	68	17-Aug-1989	207.1
23-Jul-2002	221.8	69	11-Jun-1991	206.4
24-Aug-2002	214.0	70	22-Aug-1996	206.2
18-Mar-2003	211.2	71	18-Aug-1998	202.5
28-May-2003	220.4	72	11-Mar-1996	202.1
16-Jun-2003	226.4	73	22-Oct-1989	201.8
28-Oct-2003	225.9	74	29-Aug-1994	201.8
2-Nov-2003	217.9	75	16-Jan-1986	201.6

Table 2. Instances of flares where  $X_{\text{hf}} > 200.0$ , the left side of table is sorted by date, the right is sorted by  $X_{\text{hf}}$ .

## Inter-Comparisons of GOES Satellites

The XRS (X-Ray Sensor) measurements from each GOES satellite is calibrated to one or two prior GOES satellites. That is, the absolute flux levels of the X-rays of GOES-12 has been calibrated to GOES-10, GOES-10 to GOES-8, and so forth; all the way back to GOES-1 when the X-ray instrument was calibrated on the ground to a known X-ray source. Naturally the question is whether there is a long-term drift introduced by doing this, especially at the lower flux levels. However, the calibration of each satellite is carefully performed for a period of at least a year when there is a flare or similar changes that provide a large dynamic range.

For our purposes, however, we are interested in making certain the background variations are verified, not just the flares. The results are acceptable: at  $X_{\text{b}10} > 350$ , the relative, the unbiased error is on the order of 2%. At  $X_{\text{b}10} = 300$ , the relative error suggests a 10% biased error from GOES-5 to GOES-12, and at  $X_{\text{b}10} = 200$ , the error increased by 20% over about 16 years. The known accumulated errors in the instruments (particularly at low fluxes) are approximately 30%, so we conclude that there is not a significant long-term calibration error. The  $X_{\text{hf}}$  variations show virtually no errors above 1%, confirming that there is no significant drift for the 18 years of data analyzed.

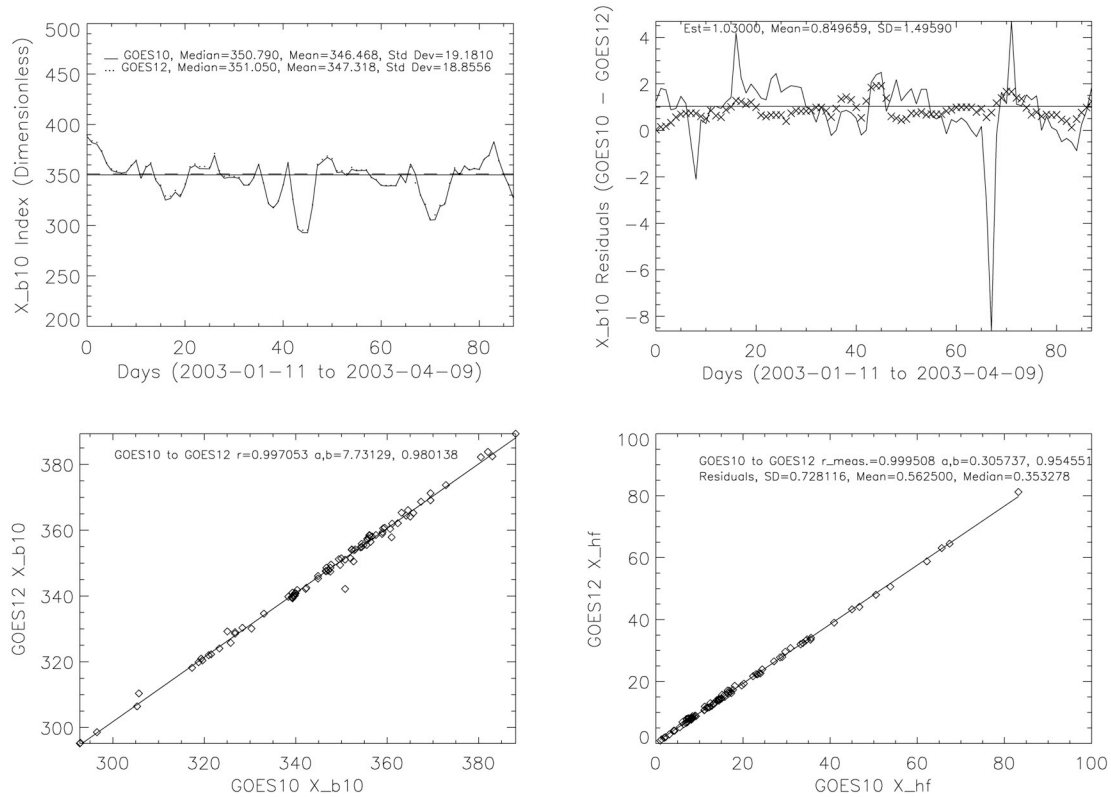


Figure 10. The linear regression between GOES-12 to GOES-10. The goodness of fit is virtually identical between all the GOES satellites at  $X_{b10} > 300$ . The upper right panel shows the residuals between GOES12 and 10 before and after an outlier is removed and the coefficients of the regression are applied. The lower left panel is the scatter plot of GOES-10 and 12, with the line showing  $GOES-12(X_{b10}) = a + b \times GOES-10(X_{b10})$ . The bottom right panel shows the correlation of the two  $X_{hf}$  indices.

Since GOES-5, each satellites time series had about a years overlap with the prior satellite, with a good dynamic range and hundreds of samples. There is one exception: GOES-8 compared to GOES-7. Because there are low-flux solar minimum conditions for the 17 months the two satellites are collecting data, there are only about 200 reliable samples for the regression. Also, there was a major change in the GOES-8 satellite and X-ray sensor as well. Beginning with GOES-8, the GOES spacecraft became 3-axis stabilized instead of the GOES 1-7 spinning satellites. The X-ray sensor was also changed by one decade to better capture flare fluxes, but at the cost of the lower decade of the instrument range, significantly degrading the ability to measure solar minimum conditions. Nevertheless, there is only a 8% standard deviation in the residuals, and there is no reason not to assume the GOES-7 to GOES-8 calibrations have significantly changed.

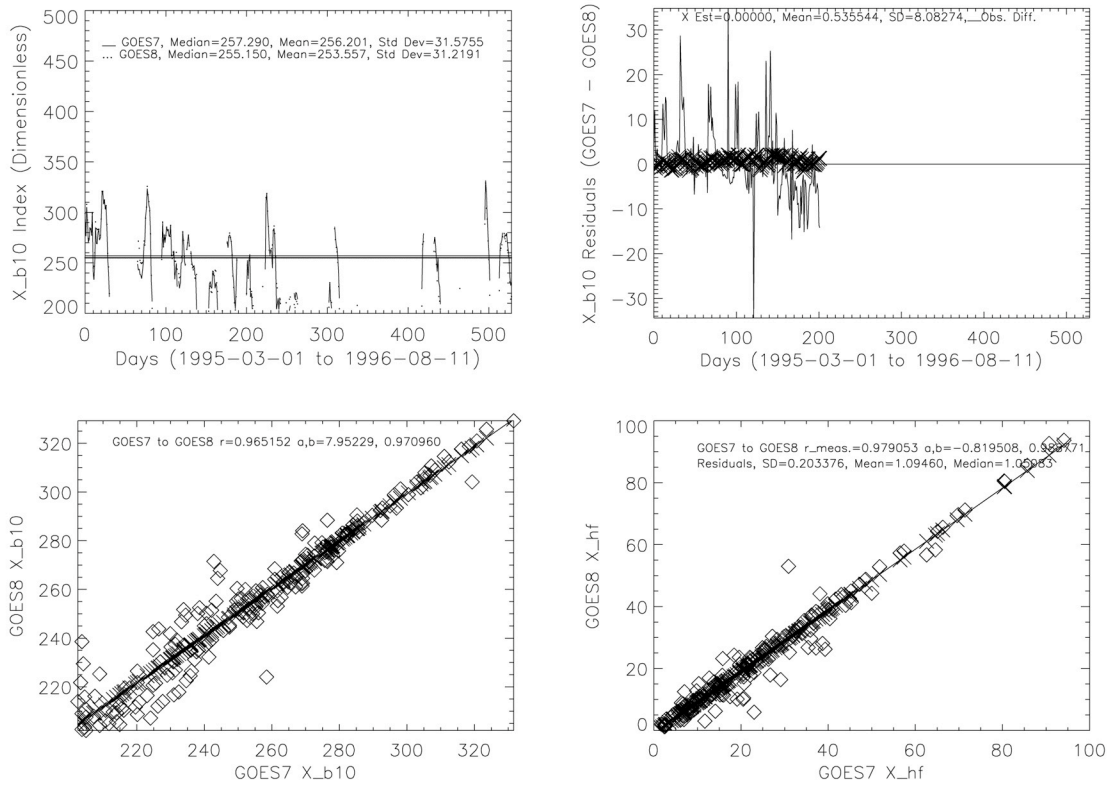


Figure 11. The linear regression between GOES-8 to GOES-7, showing to worst-case results of inter-comparing all the satellites (their figures showed extremely high correlations.) The upper left panel are the time series used (GOES-8 and 7.) The upper right panel shows the residuals between GOES-8 and 7 before and after an outlier is removed and the coefficients of the regression are applied. Because there are so many missing values between the two satellites, only about 200 samples are available and appear as a shortened time series in the plot. The lower left panel is the scatter plot of GOES-8 and 7, with the line showing  $GOES-8(X_{b10}) = a_b + b_b \times GOES-7(X_{b10})$ . The bottom right panel shows the correlation of the two sets of  $X_{hf}$  indices, also using a linear regression of  $GOES-8(X_{hf}) = a_f + b_f \times GOES-7(X_{hf})$ .

Recent analysis indicates it is possible that all the GOES X-ray data have been pre-processed with an error that resulted in the GOES 0.1-0.8 nm X-ray data being a factor 0.7 too low (oral presentation by Rodney Viereck at the 2004 Space Weather Week conference in Boulder, Colorado.) Currently efforts are underway to confirm this by comparisons with recent rocket and satellite measurements. If confirmed, one consequence is that if all the historical data are corrected, the number of historical flare C, M, and X classifications will dramatically increase as well.

## Case Study: $X_{b10}$ compared to F10.7

Often F10.7 is used as an index to coronal variations, even though the measurements contain both coronal and photospheric components. The 0.1-0.8 nm X-ray fluxes are almost entirely coronal in nature. How well can we estimate the  $F10.7_{obs}$  from daily background or median X-index values? Dick Donnelly was first to compare X-ray flux to F10.7 to show how the two behaved on time scales of a solar rotation (R. F. Donnelly, "Comparison of nonflare solar soft X ray flux with 10.7 cm flux", J. Geophys. Res. 87, 6331-6334, 1982). For this analysis, the entire period of January 1986 through May 2004 was chosen. The correlation coefficient of  $F10.7_{obs}$  and  $X_{b10}$  data is 0.8186 prior to modeling. Recall that  $X_{b10}$  is calculated by selecting the day's minimum value of the hourly lowest decile. Using  $X_{b10}$  and  $F10.7_{obs}$  in a 4-term polynomial regression results in a residual standard deviation of 38.9141, with clear low-flux effects in both  $F10.7_{obs}$  and  $X_{b10}$ . However, there is a sufficiently good correlation so that a pseudo-F10.7 (denoted  $F_X$ ) based on  $X_{b10}$  can be derived based on the following equation:

$$F_X = 47.9282 - 0.63102 X_{b10} - 4.4789 \cdot 10^3 X_{b10}^2 + 9.5324 \cdot 10^6 X_{b10}^3 \quad (3)$$

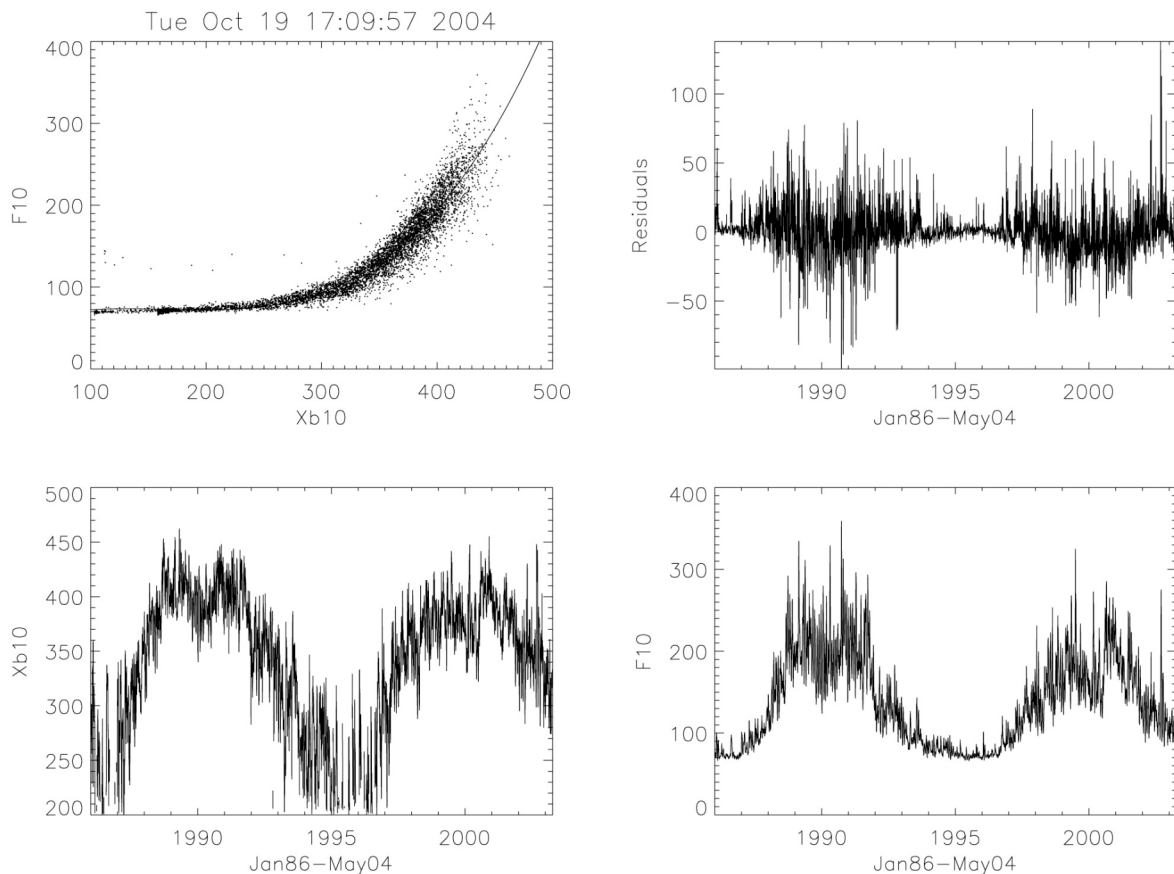


Figure 12. The 3-term regression estimating the observed  $F10.7_{obs}$  from  $X_{b10}$ . The two top panels show the scatter diagram of  $X_{b10}$  and  $F10.7_{obs}$ , and the residuals of the modeled and measured  $X_{b10}$ . The two bottom panels are the time series of the daily  $X_{b10}$  and  $F10.7_{obs}$ .

As a sidebar, comparisons to  $F10.7_{\text{obs}}$  with  $X_b$ ,  $X_{\text{mean}}$ ,  $X_{\text{median}}$ , and  $X_{\text{hf}} + X_{b10}$  showed little or no improvement in the correlations. Important differences between  $X_{b10}$  and  $F10.7_{\text{obs}}$  are apparent in figure 12: A solar-cycle effect in  $F10.7_{\text{obs}}$  shows very little variation at solar min., and the scatter at solar maximum significantly increases. What causes the differences between  $F10.7_{\text{obs}}$  and  $X_{b10}$ ? A comparison of X rays with other solar indices on solar-rotation time scales was first presented by Donnelly et al. in 1982, (R. F. Donnelly, D. F. Heath, J. L. Lean, “Active-Region Evolution and Solar Rotation Variations in Solar UV Irradiance, Total Solar Irradiance, and Soft X rays”, J. Geophys. Res., 87, A12, 10,318-10,324, 1982). When we look at the Oct.-Nov. 2003 timeframe, the effects of a single large active region in X-ray and F10.7 are apparent. It can be shown many other solar indices appear similar to sinusoidal-type variation seen in F10.7, which is due to solar rotational variations and the optical thickness of the solar atmosphere (i.e., from our terrestrial viewpoint the Central-Meridian Distance – CMD). In a nutshell, figure 13 shows why many solar indices do not compare well to X-ray fluxes on day-to-day timescales.

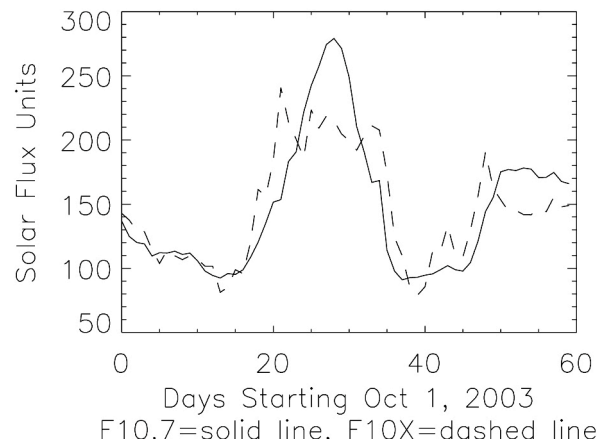


Figure 13. The observed F10.7 and the  $F10_X$  estimated from  $X_{b10}$  for October, 2003.

## Case Study: The Halloween Flares

One important observation in  $X_{b10}$  and  $X_{hf}$  is that the big X-ray flares reported during the dramatic “Halloween 2003” time period were due to an unusually high background, and not the size of the flares. In fact, there were much bigger flares in  $X_{hf}$  during other parts of the solar cycle.

Figure 14 below shows a close-up view of how the  $X_{b10}$  and  $X_{hf}$  indices vary on daily and hourly timescales. While the distinction between what is a flare and what is the background is fuzzy, at about the 80% level, it appears this technique does a good job in selecting the minimum values like one would tend to visually select the background to identify a flare. Since the algorithm for deriving  $X_{b10}$  is from the minimum of the days hourly lower decile values, and  $X_{hf}$  is based on the median for each hour, we are virtually guaranteed  $X_{b10}$  will be lower than the sum of  $X_{hf}$  and  $X_{b10}$ .

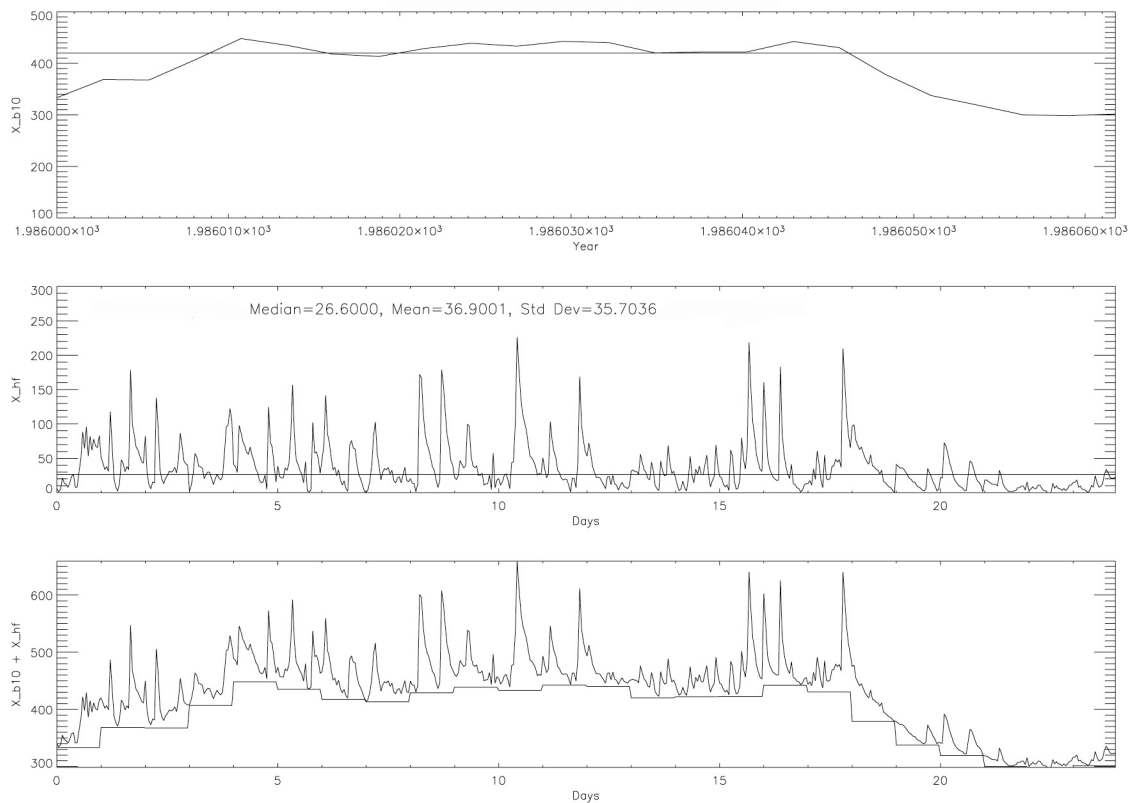


Figure 14.

If we define an  $X_{hf}$  flare as the value of  $X_{hf}$  above 200 X-index SFU’s, only two flares stand out during the Oct 18, 2003 to Nov 10, 2003.

Year	Month	Day	Hour	$X_{hf}$
2003	10	28	10	225.9
2003	11	2	16	218.4

Table 3.  $X_{hf} > 200$  (Major X-type flare classes), Halloween 2003 period.

While the SEC X-ray flare classifications (i.e., C, M, and X) are based on the 1-minute 1-8 Å values, we can approximate the classifications for the largest flares by using an hourly median X-ray index. From this view, x-class flares (when  $X_{\text{hf}} + X_{\text{b10}}$  is above 600 SFU's.) are more frequent:

Year	Month	Day	Hour	X_bf
2003	10	26	5	600.9
2003	10	26	17	607.6
<b>2003</b>	<b>10</b>	<b>28</b>	<b>11</b>	<b>659.3</b>
2003	10	28	11	600.9
<b>2003</b>	<b>11</b>	<b>2</b>	<b>16</b>	<b>640.7</b>
2003	11	3	9	609.7
2003	11	4	20	639.8

Table 4.  $X_{\text{hf}} + X_{\text{b10}} > 600$  (Hourly X-class flares), Oct 18, 2003 to Nov 10, 2003 period.

## Conclusions

One utility of our approach is that from a thermospheric/ionospheric viewpoint, dramatic relative changes in solar ionizing irradiances above the gradual day-to-day variations are often needed, as opposed to the absolute fluxes (e.g., TEC variations that last on the order of an hour). Conversely, the longer duration of day-to-day variations may have implications to the more gradual thermospheric changes (e.g., thermospheric heating, recombination, winds, etc.).

Overall, in the  $X_{b10}$  time series, it appears active region last about 4.5 solar rotations (120-days), as are the rotational effects of 1-2 active regions (with a characteristic X-ray “square wave” as an active region rotates across the disk). If a yearly average is performed on the  $X_{b10}$  time series, the 120-day active region variations are averaged out, resulting in a relatively constant  $X_{b10} = 350$  average during 1999-2003.

A surprising result is that when flares ( $X_{hf}$ ) are defined here as the sudden, large increases in flux above the background  $X_b$ , then the size of the flares (but not the frequency) are independent of the solar cycle. In other words, flares above a background level are just as large near solar minimum as solar maximum. Additionally, flares occur randomly in time, except during solar maximum flares are more frequent compared to solar minimum.

Recent analysis indicates it is possible that all the GOES X-ray data have been pre-processed with an error that resulted in the GOES 0.1-0.8 nm X-ray data being a factor 0.7 too low (oral presentation by Rodney Viereck at the 2004 Space Weather Week conference in Boulder, Colorado.) Currently efforts are underway to confirm this by comparisons with recent rocket and satellite measurements. If confirmed, one consequence is that if all the historical data are corrected, the number of historical flare C, M, and X classifications will dramatically increase as well.

## Appendix A. Glossary

$\Phi_{1-8}$	The 0.1-0.8 nm X-ray flux in $\text{W}/\text{m}^2$ .
$F10_X$	The estimated F10.7 flux from $X_{b10}$ (see eqn. 3)
FITS	Flexible Image Transport System
$X_i$	The X-ray index, calculated from the expression $X_i = 100 \times \log(\Phi_{1-8} \times 10^{10})$ .
$X_b$	The original X-ray background as reported by Bouwer et. al. NOAA Technical Memorandum (ERL SEL-62), 1982. This background uses a derivation based on the minimum hourly average of $\Phi_{1-8}$ from one of the eight-hour segments of the day.
$X_{b10}$	The new X-ray background, based on a derivation using the minimum of the day's hourly deciles.
$X_{hf}$	The hourly flare index, based on a derivation using the difference between the hourly median and hourly decile.
$X_{bf}$	The hourly flare index plus the daily $X_{b10}$ .
CMD	Central-Meridian Distance
GOES	Geosynchronous Orbiting Environmental Satellite
GPS	Global Positioning System
NOAA	National Oceanic and Atmospheric Administration
NGDC	National Geophysical Data Center
SEC	Space Environment Center
SEM	Space Environment Monitor
SET	Space Environment Technologies
SMS	Synchronous Meteorological Satellite
TEC	Total Electron Content
TR	Technical Report
XRS	X-Ray Sensor
XUV	Soft X-rays
EUV	Extreme Ultra-Violet

## Acknowledgements

Lorne Matheson of NOAA Space Environment Center was crucial to checking the accuracy of this technical report, based on his extensive experience with the GOES SEM instruments. W. Kent Tobiska of SET was extremely supportive in the development of this research and development, and was instrumental in implementing it as a solar flare prediction tool.

